INTERNATIONAL JOURNAL FOR NUMERICAL METHODS IN FLUIDS
Int. J. Numer. Meth. Fluids 2002; **39**:497–515 (DOI: 10.1002/fld.341)

Comparison of direct numerical simulations of turbulent flames using compressible or low-Mach number formulations

J. de Charentenay[1,2], D. Thévenin[2,†] and B. Zamuner[1]

[1] *ONERA, 29, Avenue de la Division Leclerc, BP 72, F-92322 Châtillon, France*
[2] *Laboratoire d'Energétique EM2C, Ecole Centrale Paris and CNRS, Grande Voie des Vignes, F-92295 Châtenay-Malabry, France*

SUMMARY

Modelling turbulent flames with an acceptable accuracy remains an open problem. In order to progress in our understanding of turbulent combustion, direct numerical simulations have been extensively employed during the last decade. These direct simulations generally rely on a fully compressible formulation, leading to extremely small time-steps associated with the propagation of acoustic waves. But, for many practical applications, acoustic phenomena are not essential. Using an incompressible approach while taking into account a dilatation term should then be much more efficient in terms of computing time. In this article we want to investigate this point by comparing results of direct simulations relying either on the compressible equations or on the low-Mach number formulation. We employ in both cases detailed models to describe chemistry and transport, in order to obtain an accurate description of the reaction zones. Two test-cases are considered for the evaluation of the low-Mach number approximation. We first compute the evolution of homogeneous isotropic turbulence decaying with time, without chemical reactions. In the second case a turbulent premixed ozone flame is investigated. For both configurations the computing time associated with the low-Mach number simulation is at least an order of magnitude shorter, while keeping a similar accuracy for the flame properties. This demonstrates that the low-Mach number formulation is extremely efficient and suitable to investigate the detailed structure of turbulent flames when acoustic phenomena are not of primary interest. Copyright © 2002 John Wiley & Sons, Ltd.

KEY WORDS: DNS; low-Mach number; turbulence; detailed chemistry; Poisson equation

INTRODUCTION

The development of accurate models for computing turbulent flames implies a detailed investigation of the intrinsic features controlling the coupling between turbulence and chemical reactions. One of the best tools presently available for such investigations is direct numerical simulation (DNS). DNS has been widely used in the last decade to provide reliable information needed for a better modelling [1–4]. The main problem of these direct computations

* Correspondence to: D. Thevenin, Laboratoire d'Energétique EM2C, UPR 288 du CNRS, Ecole Centrale Paris, Grande Voie des Vignes, F-92295 Châtenay-Malabry Cedex, France
† E-mail: thevenin@em2c.ecp.fr

Received February 2001
Revised November 2001

comes from the fact that they have to take into account a wide range of time-scales. In particular, DNS of the compressible Navier–Stokes equations (by far the most frequent ones in reacting flow studies) consider the very fast propagation of acoustic waves through the numerical domain. Simultaneously, they have to cope with chemical time-scales, comprising not only very fast reactions between intermediate species but also quite slow processes associated, for example, with pollutant formation [5]. These contradictory requirements lead to extremely high computing times for DNS of reacting flows and therefore strongly limit their possible usage to improve our understanding of turbulent combustion [6].

In this work we explore one possible way to reduce the computational times associated with DNS. This possible acceleration comes from the observation that studies of turbulent combustion are not focused on acoustic phenomena. In particular, we observed that in many cases the combustion process happens at low-Mach numbers. In this specific configuration the pressure in the flow is nearly uniform and the coupling between the fluctuating pressure and the density can be neglected. Therefore, the system of equations based on this observation does not have to take into account acoustic waves.

Of course, the use of this approximation for combustion applications raises up the problem of the coupling between acoustics and chemical reactions. Prasad [7] has previously shown that the pressure waves are very sensitive to the reaction zone, but that the flame structure remains unchanged if only isolated acoustic perturbations are considered, even for high amplitudes. In the case of flows at low-Mach numbers, the amplitude of the pressure perturbation is very small. Moreover, for DNS, the geometry is generally open, reducing the intensity of acoustic coupling. We therefore think *a priori* that the low-Mach number approach could be successfully applied to investigate in detail the structure of turbulent flames, and we will check this point in what follows.

Several works have already been published concerning the possibility of speeding-up flow computations by modifying the acoustic phenomena [8, 9]. These methods reduce the acoustic speed by a given factor and thereby increase artificially the Mach number by a similar value, leading to a more efficient numerical integration. In this case, the compressible nature of the equations is conserved but the amplitude of the acoustic waves is increased. Similar artificial modifications of the velocity of acoustic waves have also been used more recently to speed-up steady-state computations of reacting flows [10, 11].

In the present study, we consider an incompressible but dilatable approach, which leads us to neglect completely all acoustic waves inside the computational domain. This formulation has been first used for non-reacting flows [12] and is of course only valid at low-Mach numbers. Again this limitation is not a problem for many interesting configurations. This incompressible dilatable formulation has been later on extended to reacting flows [13] and has already been successfully compared to a compressible approach using simple chemistry [14]. The basic technique is the same for reacting and non-reacting flows. The pressure is divided into a spatially homogeneous part $p_0(t)$ and a dynamic fluctuating part $\tilde{p}(\boldsymbol{x},t)$. It can be proved that, in the low-Mach number limit, $\tilde{p}(\boldsymbol{x},t)$ is very small compared to $p_0(t)$. We will explain this splitting in more detail in a later section. The resulting equations contain vorticity and entropy waves, but acoustic waves have disappeared. Therefore the time-step is no longer limited by acoustic times, but by characteristic convection, diffusion or reaction times, which can be orders of magnitude larger. This approach has been successfully applied to chemically reacting flows using fully implicit or semi-implicit algorithms in more recent time-dependent simulations. For example, planar or axisymmetric jet flames showing coherent

instabilities [15–17] and the interaction between a flame and an isolated vortex [18, 19] have been investigated in great detail. It was always observed that, in agreement with theoretical predictions, the low-Mach number approximation reduces the stiffness of the system and leads to considerably shorter computing times.

In the present work we want to assess the interest of this low-Mach number formulation for DNS of turbulent flames using detailed chemistry. In order to do so we will compare the results of two different time-dependent computations, both involving detailed models to describe chemistry and transport processes. The first result, considered as a reference, corresponds to a DNS using the fully compressible Navier–Stokes equations, obtained with the code *Parcomb*. A second code has been derived from this first one using similar numerical techniques but based on the low-Mach number approximation. In this second code we neglect acoustic waves and the coupling of acoustics with chemical reactions. Since reactive/diffusive phenomena are equally well taken into account, and considering that the spatial and temporal accuracy of the numerical solution is still very high, we will call this second approach direct low-Mach number simulation (DLMNS) in the following. By comparing the accuracy of the obtained results, we will see that the two formulations are equivalent in the domain of validity of the low-Mach number approximation.

This paper has been organized as follows. In the first section the numerical and physical models are presented. We introduce both the compressible equations and the low-Mach number formulation. We then present the results of two test-cases. In the first case we examine the time-dependent evolution of a field of homogeneous isotropic turbulence. We show that the low-Mach algorithm is able to reproduce with a very good level of accuracy the coupling between pressure and velocity. We afterwards compute a turbulent premixed ozone flame using a detailed reaction scheme. The advantage of considering ozone chemistry is that it contains relatively slow characteristic time-scales, so that the reactive terms can be integrated in time with a fully explicit scheme while keeping large time-steps. Here again the behaviour of the flame front interacting with the turbulence is accurately reproduced using the low-Mach number assumption. We finally give some details concerning computing times and the origin of the slight differences observed between DNS and DLMNS results. We conclude that DLMNS results are of comparable accuracy to those obtained with DNS. But since the low-Mach number code is no longer limited by the acoustic time-step restriction, a considerable speed-up is obtained.

NUMERICAL AND PHYSICAL MODELS

Governing equations

For DNSs reactive flows are generally described by using the compressible multi-species Navier–Stokes equations [20, 21]:

$$\partial_t \rho + \nabla \cdot (\rho \boldsymbol{v}) = 0 \tag{1a}$$

$$\partial_t (\rho Y_k) + \nabla \cdot (\rho \boldsymbol{v} Y_k) + \nabla \cdot \boldsymbol{F}_k = M_k \omega_k \quad (k = 1, \ldots, N_s) \tag{1b}$$

$$\partial_t (\rho \boldsymbol{v}) + \nabla \cdot (\rho \boldsymbol{v} \otimes \boldsymbol{v}) + \nabla \cdot \underline{\underline{\tau}} = -\nabla p \tag{1c}$$

$$\partial_t (\rho e_t) + \nabla \cdot (\rho \boldsymbol{v} e_t) + \nabla \cdot \boldsymbol{Q} = -\nabla \cdot (p \boldsymbol{v}) - \nabla \cdot (\underline{\underline{\tau}} \cdot \boldsymbol{v}) \tag{1d}$$

using following definitions:

$$p = \frac{\rho R_0 T}{M}$$

$$e_t = \tfrac{1}{2}(\boldsymbol{v}\cdot\boldsymbol{v}) + h - \frac{p}{\rho}$$

$$\boldsymbol{Q} = -\lambda \boldsymbol{\nabla} T + \sum_{k=1}^{N_s} (h_k \boldsymbol{F}_k)$$

$$\underline{\underline{\tau}} = \tfrac{2}{3}\mu(\boldsymbol{\nabla}\cdot\boldsymbol{v})\boldsymbol{I} - \mu(\boldsymbol{\nabla}\boldsymbol{v} + (\boldsymbol{\nabla}\boldsymbol{v})^t)$$

where ρ represents the density, $\boldsymbol{v}$ the velocity vector, Y_k the mass fraction of species k, $\boldsymbol{F}_k$ the species diffusion flux, M_k the molar mass, ω_k the molar production rate, N_s the total number of species in the flow, p the pressure, $\underline{\underline{\tau}}$ the viscous strain tensor, e_t the specific total energy, $\boldsymbol{Q}$ the heat flux, λ the thermal conductivity, h_k the specific enthalpy of species k, R_0 the perfect gas constant, T the temperature, M the mixture molar mass, h the mixture specific enthalpy and μ the dynamic viscosity. Equations (1a)–(1d) describe, respectively, the conservation of mass, species, momentum and energy. In fact it is possible to suppress one of the N_s equations in Equation (1b), since the sum of all these equations corresponds to Equation (1a).

Chemical source terms and transport properties

Thermodynamics, transport properties and chemical source terms are computed in both codes using existing available libraries, described in detail in various publications [22–25]. We therefore restrain ourselves to a brief summary.

The chemical kinetic scheme is described using the following form:

$$\sum_{k=1}^{N_s} \nu_{ki}^{f} S_k \leftrightarrows \sum_{k=1}^{N_s} \nu_{ki}^{b} S_k \quad (i = 1, \ldots, N_r)$$

where N_r is the total number of reactions, ν_{ki}^{f} and ν_{ki}^{b} the forward and backward stoichiometric coefficients, and S_k the species symbols. The molar production rate of species k is then computed by

$$\omega_k = \sum_{i=1}^{N_r} (\nu_{ki}^{b} - \nu_{ki}^{f}) q_i$$

where q_i is the rate of progress of reaction i, whose expression (without third body) is

$$q_i = K_{fi} \prod_{k=1}^{N_s} c_k^{\nu_{ki}^{f}} - K_{bi} \prod_{k=1}^{N_s} c_k^{\nu_{ki}^{b}}$$

where c_k is the molar concentration of species k, K_{fi} and K_{bi} the forward and backward rate constants of reaction i. The rate constants K_{fi} and K_{ri} are evaluated by considering an Arrhenius law and the equilibrium constant is given by thermodynamics. By modifying slightly this expression, it is also possible to take into account third bodies with different

efficiencies [22]. All the Arrhenius parameters and the thermodynamic constants are found in the literature. More details can be found in References [21–23].

We now explain the computation of the diffusion terms. Neglecting the Soret and Dufour effects, the expression of the species fluxes $\boldsymbol{F}_k$ becomes

$$\boldsymbol{F}_k = -\sum_{l=1}^{N_s} \rho \widetilde{D_{kl}} \boldsymbol{\nabla} X_k$$

where $\widetilde{D_{kl}}$ are the multi-species diffusion coefficients and X_k the molar fraction of species k. In order to reduce computation time [24, 25], we only take into account the diagonal terms of the multi-species diffusion coefficient matrix and add a correction velocity $\boldsymbol{V}_{\text{corr}}$ to ensure mass conservation. This treatment leads to

$$\boldsymbol{F}_k = -\rho Y_k \frac{D_{k,\text{m}}}{X_k} \boldsymbol{\nabla} X_k - \rho Y_k \boldsymbol{V}_{\text{corr}}$$

where $D_{k,\text{m}}$ are the projection of the multi-species diffusion coefficients. The correction velocity $\boldsymbol{V}_{\text{corr}}$ is given by

$$\boldsymbol{V}_{\text{corr}} = -\sum_{k=1}^{N_s} Y_k \frac{D_{k,\text{m}}}{X_k} \boldsymbol{\nabla} X_k$$

This formulation is a realistic approximation to the multi-component transport properties [24, 25] and is used in both our compressible and low-Mach number simulations. In the future we will try to implement more accurate transport models [26] in order to take into account the whole matrix of binary diffusion coefficients, including Soret and Dufour effects. Nevertheless, since we use the same description of the reactive and diffusive processes in both codes, these models should not change anything for the comparisons we want to undertake here.

Low-Mach number approximation

For many applications relying on combustion, practical devices are operated at low flow speeds and very low Mach numbers. When trying to simulate such configurations with DNS codes, an explicit time integration of Equations (1a)–(1d) leads to severe time-step limitations corresponding to the most critical time-scale. This fastest characteristic time-scale is associated with the propagation of acoustic waves, leading to a wave velocity equal to the maximum of the flow speed plus the local velocity of sound. Using compressible equations for very low-Mach numbers cases is then particularly inefficient [27, 28]. It is much better to consider a low-Mach number approximation, which enables us to solve only the vorticity and entropy waves and neglect the acoustic ones. The derivation of the low-Mach number equations is performed through an asymptotic expansion of the non-dimensional variables in terms of the Mach number M [13]:

$$p^* = p_0^* + M p_1^* + \gamma M^2 p_2^* + o(M^3) \tag{2a}$$

$$\boldsymbol{v}^* = \boldsymbol{v}_0^* + M \boldsymbol{v}_1^* + o(M^2) \tag{2b}$$

$$T^* = T_0^* + M T_1^* + o(M^2) \tag{2c}$$

where $(.)^*$ is the corresponding non-dimensional variable. Expansions (2a)–(2c) are introduced in the non-dimensional compressible equations and the terms of equal power of M are gathered together. It turns out that the pressure p can be split into a spatially uniform pressure $p_0(t)$ and a dynamic perturbation part $\tilde{p}(\boldsymbol{x},t)$. Using this decomposition the equations for combustion at zero-Mach number can be established [21], leading to

$$\partial_t \rho + \boldsymbol{\nabla}\cdot(\rho \boldsymbol{v}) = 0 \tag{3a}$$

$$\partial_t(\rho Y_k) + \boldsymbol{\nabla}\cdot(\rho \boldsymbol{v} Y_k) + \boldsymbol{\nabla}\cdot\boldsymbol{F}_k = M_k\omega_k \quad (k=1,\ldots,N_s) \tag{3b}$$

$$\partial_t(\rho \boldsymbol{v}) + \boldsymbol{\nabla}\cdot(\rho \boldsymbol{v}\otimes\boldsymbol{v}) + \boldsymbol{\nabla}\cdot\underline{\underline{\tau}} = -\boldsymbol{\nabla}\tilde{p} \tag{3c}$$

$$\partial_t(\rho e_t) + \boldsymbol{\nabla}\cdot(\rho \boldsymbol{v} e_t) + \boldsymbol{\nabla}\cdot\boldsymbol{Q} = 0 \tag{3d}$$

In order to simplify the computational algorithm, it is useful to employ primitive variables for the species equations (3b). In the same way it is easier to solve a temperature equation instead of the energy equation (3d). The derivation of the following isobaric temperature equation is again achieved by introducing the asymptotic expansions (2a)–(2c) in the compressible temperature equation:

$$\rho C_p \partial_t T + \rho C_p \boldsymbol{v}\cdot\boldsymbol{\nabla}T + \boldsymbol{\nabla}\cdot\left(\boldsymbol{Q} - \sum_{k=1}^{N_s}(h_k\boldsymbol{F}_k)\right)$$
$$= -\sum_{k=1}^{N_s}(c_{p_k}\boldsymbol{F}_k\cdot\boldsymbol{\nabla}T) - \sum_{k=1}^{N_s}(M_k\omega_k h_k) \tag{3e}$$

Note that the low-Mach number approximation leads to the disappearance of the viscous and pressure terms in the energy equation (3d) and temperature equation (3e). This is due to the fact that the kinetic energy is not of the same order of magnitude as the internal energy in terms of Mach number. The pressure splitting is also introduced in the state law for perfect gas, which becomes

$$p_0 = \frac{\rho R_0 T}{M}$$

It can be seen in this equation that we therefore suppress the coupling between the fluctuating pressure $\tilde{p}$ and the density. As a consequence, the Euler system is modified and acoustic waves are neglected. A specific procedure is now required to determine the hydrodynamic perturbation $\tilde{p}(\boldsymbol{x},t)$. Several possibilities has been proposed in previous publications. We decide to use a pressure-projection method [12–14], which leads to solve Equation (3c) in two consecutive parts. In a first step, it is integrated considering a constant pressure, leading to Equation (4a). Afterwards, the pressure perturbation $\tilde{p}(\boldsymbol{x},t)$ is determined before performing the second integration step, corresponding to equation (4b):

$$(\rho \boldsymbol{v})^* = (\rho \boldsymbol{v})^n + \Delta t[-\boldsymbol{\nabla}\cdot(\rho \boldsymbol{v}\otimes\boldsymbol{v}) - \boldsymbol{\nabla}\cdot\underline{\underline{\tau}}] \tag{4a}$$

$$(\rho \boldsymbol{v})^{n+1} = (\rho \boldsymbol{v})^* + \Delta t[-\boldsymbol{\nabla}\tilde{p}] \tag{4b}$$

After solving equation (4a), we determine the pressure perturbation by taking the divergence of Equation (4b) and introducing the continuity equation (3a) to estimate $\nabla\cdot(\rho\boldsymbol{v})^{n+1}$, leading to the following Poisson equation for $\tilde{p}(\boldsymbol{x},t)$:

$$\nabla^2\tilde{p}=\frac{1}{\Delta t}((\partial_t\rho)^{n+1}+\nabla\cdot(\rho\boldsymbol{v})^*) \tag{5}$$

This methodology is an extension to reactive flows of algorithms employed for incompressible non-reactive flows [13]. The dilatation induced by heat release is taken into account through the introduction of the density variation term $(\partial_t\rho)^{n+1}$. This term is evaluated numerically in our code, using a third-order backward finite-difference formulation:

$$(\partial_t\rho)^{n+1}=\frac{1}{\Delta t}(\tfrac{11}{6}\rho^{n+1}-\tfrac{6}{2}\rho^n+\tfrac{3}{2}\rho^{n-1}-\tfrac{2}{6}\rho^{n-2})$$

In this approach the continuity equation is a constraint, which is taken into account through the dilatation term $(\partial_t\rho)^{n+1}$. It is known that the finite-difference approximation of this term can lead to numerical errors [29] and other techniques have been proposed. For example, a velocity divergence constraint can be derived from the continuity equation and introduced in a Poisson equation with variable coefficients. We do not use this more complex method here. We have observed that, in real cases involving viscous flows and thermal conductivity, the error introduced by the numerical approximation of $(\partial_t\rho)^{n+1}$ is negligible compared to the magnitude of physical effects.

The low-Mach number approximation we have presented here has been successfully applied by other authors to various reacting flows, see for example References [16, 18, 19, 30]. In the present study we wish to compare the results obtained using both the compressible equations and the low-Mach number approximation applied to DNS of turbulent flames. The compressible DNS code is used as the reference solution. The low-Mach number DLMNS code is employed for the comparisons shown below. This comparison is required to demonstrate whether or not the low-Mach number formulation can be used instead of the compressible one for such applications (turbulent combustion, slow chemistry). For these conditions, we expect that the coupling between acoustics and combustion will be very weak.

Numerical methods

The compressible DNS code *Parcomb* has already been described in detail in previous publications, see for example References [31, 32]. Equations (1a)–(1d) are solved using conservative dimensional variables. Spatial derivatives are computed with sixth-order accurate central finite-differences. Time integration is performed with a fourth-order Runge–Kutta formulation. The treatment at the boundaries is based on the NSCBC conditions for multi-species flows [33].

The low-Mach number DLMNS code uses similar numerical techniques to compute spatial derivatives and to perform time-integration. But the low-Mach number approximation leads to a two-stage integration of the momentum equation (3c), as explained in the previous section. Boundary conditions are simply given by Neumann (zero-gradient) and Dirichlet (constant value) conditions, since characteristic boundary conditions cannot be used here. The resolution of the Poisson equation for pressure is a key point of the method and is described in the next section.

Solving the Poisson equation for pressure

The global accuracy of the DLMNS results depends on the level of accuracy obtained when solving the Poisson equation for pressure. In the present study, we investigate only configurations that involve periodic and inlet/outlet boundary conditions and we use spectral methods along periodic directions.

The first test-case (time evolution of a field of turbulence) involves periodic boundary conditions in all directions. In this case, the integration of the Poisson equation is simply performed as follows:

$$\partial_{xx}^2 \tilde{p} + \partial_{yy}^2 \tilde{p} = f(x, y) \tag{6}$$

where x and y are the spatial co-ordinates and f is the source term of Equation (5). Using fast-Fourier-transformations (FFT), Equation (6) can be rewritten in the Fourier space:

$$-\lambda^2 \hat{\tilde{p}} - \eta^2 \hat{\tilde{p}} = \hat{f}(\lambda, \eta) \tag{7}$$

where λ and η are the wavenumbers in the x and y directions, and $\hat{\cdot}$ denotes the Fourier transform. Equation (7) is then directly inverted in the Fourier space and transformed back to the physical space. Direct and reverse FFT's are performed using an existing library [34] with a high level of vectorization.

For the second test-case we consider the interaction between an initially planar premixed flame and a turbulence field. This requires the use of inlet and outlet boundary conditions in the streamwise direction x, while keeping periodic conditions in the spanwise direction y. We apply first a Fourier transform along y, so that Equation (6) can be written as follows:

$$\partial_{xx}^2 \hat{\tilde{p}} - \eta^2 \hat{\tilde{p}} = \hat{f}(x, \eta) \tag{8}$$

In order to solve Equation (8), the second-order derivative of the pressure perturbation along the x direction is first discretized using a fourth-order compact scheme [35] corresponding to the classical Padé approach. The low-Mach number code with this compact scheme is referred to as DLMNS-CS. A first-order finite-difference approximation is used at the boundaries (inlet—left boundary—, $\nabla \tilde{p} = 0$/outlet—right boundary—, $\tilde{p} =, 0$). We finally obtain the following discretization for an equidistant grid with spacing Δx:

$$\textit{Inlet}: \quad \frac{1}{\Delta x}\hat{\tilde{p}}_1(\eta) - \frac{1}{\Delta x}\hat{\tilde{p}}_2(\eta) = 0$$

$$\textit{Central nodes}: \quad \left(\frac{6}{5\Delta x^2} - \frac{1}{10}\eta^2\right)\hat{\tilde{p}}_{i-1}(\eta) + \left(-\frac{12}{5\Delta x^2} - \eta^2\right)\hat{\tilde{p}}_i(\eta) + \left(\frac{6}{5\Delta x^2} - \frac{1}{10}\eta^2\right)\hat{\tilde{p}}_{i+1}(\eta) = \frac{1}{10}\hat{f}_{i-1}(\eta) + \hat{f}_i(\eta) + \frac{1}{10}\hat{f}_{i+1}(\eta)$$

$$\textit{Outlet}: \quad \hat{\tilde{p}}_{nx}(\eta) = 0$$

As an alternative to the compact scheme, we have also tested a fourth-order central finite-difference scheme, identical to that employed in Reference [36]. The low-Mach number code with central finite-difference is referenced as DLMNS-FD, and corresponds to following

discretization:

$$\textit{Inlet}: \quad -\frac{3}{\Delta x}\hat{\tilde{p}}_1(\eta)+\frac{4}{\Delta x}\hat{\tilde{p}}_2(\eta)-\frac{1}{\Delta x}\hat{\tilde{p}}_3(\eta)=0$$

$$\textit{Second node}: \quad \frac{1}{\Delta x^2}\hat{\tilde{p}}_1(\eta)-\left(\frac{2}{\Delta x^2}+\eta^2\right)\hat{\tilde{p}}_2(\eta)+\frac{1}{\Delta x^2}\hat{\tilde{p}}_3(\eta)=\hat{f}_2(\eta)$$

$$\textit{Central nodes}: \quad -\frac{1}{12\Delta x^2}\hat{\tilde{p}}_{i-2}(\eta)+\frac{16}{12\Delta x^2}\hat{\tilde{p}}_{i-1}(\eta)-\left(\frac{30}{12\Delta x^2}+\eta^2\right)\hat{\tilde{p}}_i(\eta)+\frac{16}{12\Delta x^2}\hat{\tilde{p}}_{i+1}(\eta)-\frac{1}{12\Delta x^2}\hat{\tilde{p}}_{i+2}(\eta)=\hat{f}_i(\eta)$$

$$\textit{Last but one node}: \quad \frac{1}{\Delta x^2}\hat{\tilde{p}}_{nx-2}(\eta)-\left(\frac{2}{\Delta x^2}+\eta^2\right)\hat{\tilde{p}}_{nx-1}(\eta)+\frac{1}{\Delta x^2}\hat{\tilde{p}}_{nx}(\eta)=\hat{f}_{nx-1}(\eta)$$

$$\textit{Outlet}: \quad \hat{\tilde{p}}_{nx}=0$$

These systems are solved using, respectively, tri- and penta-diagonal matrix solvers [37]. It would be possible to increase further the accuracy of the resolution method for the Poisson equation by increasing the accuracy of the spatial discretization [38, 39] or by using pseudo-spectral methods. We have not tested these solutions yet, since the obtained precision appears to be sufficient for the configurations we want to investigate.

RESULTS AND COMPARISONS

Time-dependent evolution of freely decaying turbulence

As a first test-case we consider the evolution of a two-dimensional field of homogeneous isotropic turbulence. The turbulence field is initialized using a von Kármán spectrum with Pao correction for near-dissipation scales [40]:

$$E(k)=A\frac{(\overline{u'^2})^{5/2}}{\varepsilon_d}\frac{(k/k_e)^4}{[1+(k/k_e)^2]^{17/6}}\exp\left[-\frac{3}{2}\alpha\left(\frac{k}{k_d}\right)^{4/3}\right]$$

In the above formula, A and α are constants, ε_d is the dissipation value, k_e and k_d, respectively, the wavelengths of the maximum of turbulent kinetic energy and dissipation. The velocity fluctuations are considered to be uncorrelated, so that the velocity phase is given by a random number generator. The generation of this field of pseudo-turbulence takes place in the Fourier space. An inverse FFT is then applied to compute the turbulent velocity field in the real, physical space.

For the results presented in this paper, the initial field of turbulence corresponds to a random-mean-square turbulent velocity of $u'=3$ m/s and an integral length-scale of $\Lambda=0.68$ mm, leading to a Reynolds number of 133 for pure air at 300 K and atmospheric pressure. The corresponding peak Mach number is about 0.01. The present conditions are therefore in the domain of validity of the low-Mach number approximation.

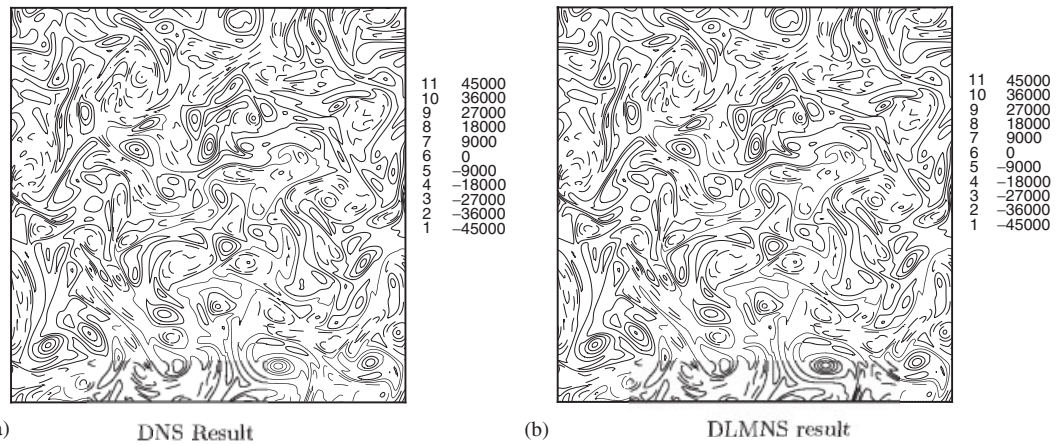

Figure 1. Isolevels of vorticity at $t=2\tau$. Solid lines represent positive values, long dashed lines negative values. Results obtained with the DNS code (a) and with the DLMNS code (b).

The size of the computational domain is $1\,\text{cm}\times 1\,\text{cm}$, discretized with a mesh of 251×251 points, leading to a constant grid size of $40\mu\text{m}$. It is clear that such computations should ideally be carried out in three dimensions. The behaviour of two-dimensional turbulence is different from that observed in more realistic three-dimensional computations [41]. But, again, we only want to compare here results obtained for the same configuration with two different codes. We do not intend to give any conclusion concerning the evolution of turbulence itself. We therefore consider that this two-dimensional computation is a good test-case to identify possible differences between the two different approaches employed in the two codes. It must be kept in mind that direct simulations of reacting flows using detailed models for chemistry and transport are still extremely expensive, and cannot possibly be carried out in three dimensions on present computers, even if this particular non-reacting test-case could easily be carried out in 3D.

Results are presented for a time $t=2\tau$, where $\tau=\Lambda/u'=0.226\,\text{ms}$ is the characteristic time of the large turbulent structures. The vorticity field obtained with the DNS code is shown in Figure 1(a). This result is very similar to that given by the DLMNS code, shown in Figure 1(b). The observed discrepancies are very small. For example, the relative difference is everywhere lower than 2% for the vorticity. These small differences are probably due to the acoustic waves observed in the DNS simulation and neglected in the DLMNS computation. Since the analytical formulation of the initial energy spectrum does not correspond to an exact solution of the compressible equations, the initial conditions imposed in the two codes tend to generate weak acoustic waves. These waves propagate through the periodic domain in the compressible simulation and induce the small differences observed.

The initial spectrum of turbulent energy (Figure 2) reproduces the classical $k^{-5/3}$ energy decay for intermediate wave numbers. The energy spectra obtained with DNS and DLMNS are identical at $t=2\tau$, as shown in Figure 2. The observed turbulence decay is close to k^{-4}, in agreement with previously observed two-dimensional results [42]. This proves that the pressure-projection method is able to reproduce correctly the pressure–velocity coupling and to capture entropy waves. The perturbation pressure $\tilde{p}(\boldsymbol{x},t)$ obtained using the DLMNS

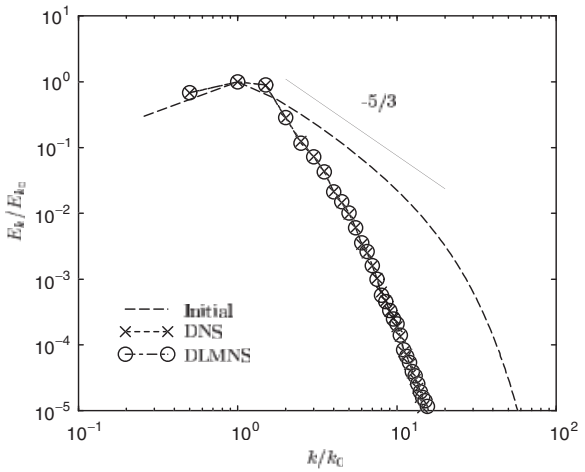

Figure 2. Energy spectrum of the turbulence field at time $t=0$ (dashed line) and $t=2\tau$ computed with the DNS code (short dashed line and crosses) and the DLMNS code (dashed–dotted line and circles).

code shows a very small amplitude, close to 1 Pa, as expected. This non-reactive test-case demonstrates that the low-Mach number approximation can be used to simulate accurately the time-evolution of a freely decaying turbulence field using DNS.

Moreover, we observe that the computing time is reduced tremendously when using the low-Mach number approach. In the present computations the time-step corresponding to a CFL value of 0.8 is $\Delta t|_{\mathrm{CFL}}=8.9\times10^{-8}$ s and is used as the time-step for the DNS code. The time-step employed within the DLMNS code corresponds to a stability criterion associated with the viscous terms, given here by $\Delta t|_{\mathrm{FOU}}=5\times10^{-6}$ s for a Fourier number of 0.1. The time-step used during the DLMNS computation is therefore 56 times larger than the time-step used during the DNS computation. Both simulations have been performed on a scalar computer *SUN Enterprise 450*. The computation time needed for the DLMNS simulation is 12 times shorter than the CPU time of the corresponding DNS. This speed-up factor is smaller than the time-step increase, since the numerical methods involved by the DLMNS computations lead to a higher CPU cost per iteration. Nevertheless, this very large acceleration factor shows the potential interest of the low-Mach number assumption for the investigation of turbulent configurations using direct simulations. We now have to check the accuracy of this method for reacting flows.

Structure of a turbulent ozone flame

As a second step we compare the results obtained with the compressible DNS and with the low-Mach number DLMNS for a turbulent premixed ozone flame. Previous authors have pointed out that problems could be theoretically observed with the low-Mach number approximation for very fast kinetics and closed domains. In this case a coupling between acoustics and chemical reactions could lead to a failure of the low-Mach number hypothesis [43, 44]. Due to this fact, and since our time integration procedure is still fully explicit, we restrict ourselves in this first study to ozone flames. It is well known that the chemical processes

Table I. Chemical mechanism employed for the ozone flame.

	Reaction	A (cm,mol,s)	b	E (kJ/mol)
(1)	$O_3 + O_3 \rightarrow O_2 + O + O_3$	3.4×10^{18}	-1.25	96.3
(2)	$O_3 + O_2 \rightarrow O_2 + O + O_2$	1.5×10^{18}	-1.25	96.3
(3)	$O + O_2 + O_2 \rightarrow O_3 + O_2$	1.7×10^{13}	0	-8.8
(4)	$O + O_2 + O_3 \rightarrow O_3 + O_3$	7.4×10^{12}	0	-8.8
(5)	$O + O_3 \rightarrow O_2 + O_2$	2.3×10^{13}	0	21.8
(6)	$O + O + O_2 \rightarrow O_2 + O_2$	1.4×10^{18}	-1	1.4
(7)	$O + O + O \rightarrow O_2 + O$	4.0×10^{18}	-1	1.4

(Table I) controlling ozone decomposition [45] show very slow characteristic chemical times. The slow kinetics of ozone lead to a very small acoustic-based Damköhler number. Therefore, and since we use an open domain, the low-Mach number hypothesis should be valid in this case.

As a starting solution we first compute a one-dimensional steady laminar premixed ozone flame for a fresh gas composition corresponding to a mixture of O_3 (20%) and O_2 (80% in mole fraction) at a temperature T_u equal to 300 K and a pressure of 1 bar. The computed laminar flame velocity is equal to 0.3m/s and the burnt gas temperature T_b is 1092K. The initial flame thickness δ_l, defined as $\delta_l = (T_b - T_u)/|\partial_x T|_{max}$, is equal to 0.26mm. These characteristics are in good agreement with previously published results [46]. The one-dimensional flame profiles obtained using DNS and DLMNS are shown in Figure 3. A very good agreement is observed. In this case the Mach number value is equal to 0.001 in the fresh gas and 0.002 in the burnt gas. The order of magnitude of the perturbation pressure $\tilde{p}(\boldsymbol{x}, t)$ compared to the thermodynamic pressure p_0 is $\tilde{p}/p_0 \approx 6 \times 10^{-6}$. This ratio can be correlated to the Mach number using Equation (2a) leading to the expression for pressure splitting, $\tilde{p} = \gamma M^2 p_2$. In the present case the value of $\gamma M^2 \approx 2 \times 10^{-6}$ is comparable to $\tilde{p}/p_0$, showing the coherence of the low-Mach number approximation.

In order to obtain a different comparison, we also compute the total integrated heat release rate inside the computational box. The results of DNS and DLMNS are of the same order of magnitude:

- *DLMNS results*: $H_{rDLMNS} = \int \sum_{k=1}^{N_s} (M_k \omega_k h_k) \, dl = 3.623 \times 10^5$ J/m^2 s,
- *DNS results*: $H_{rDNS} = \int \sum_{k=1}^{N_s} (M_k \omega_k h_k) \, dl = 3.510 \times 10^5$ J/m^2 s.

The observed difference of 3% comes from small changes in the high-temperature part of the flame structure, due to slightly differing velocity profiles. These velocity differences can themselves be related to the different boundary conditions employed in the two codes. The DLMNS formulation uses only zero-gradient and constant-value boundary conditions, while the DNS simulation relies on characteristic boundary conditions, where the pressure relaxes with time towards a given level [33]. It is therefore impossible to consider that both results should be exactly identical. The pressure and velocity profiles are indeed very similar in both cases, but still present small differences resulting from the different boundary conditions.

In order to start the interaction with turbulence, these one-dimensional flames are extended along the y direction and the same initial field of turbulence is superposed on the resulting

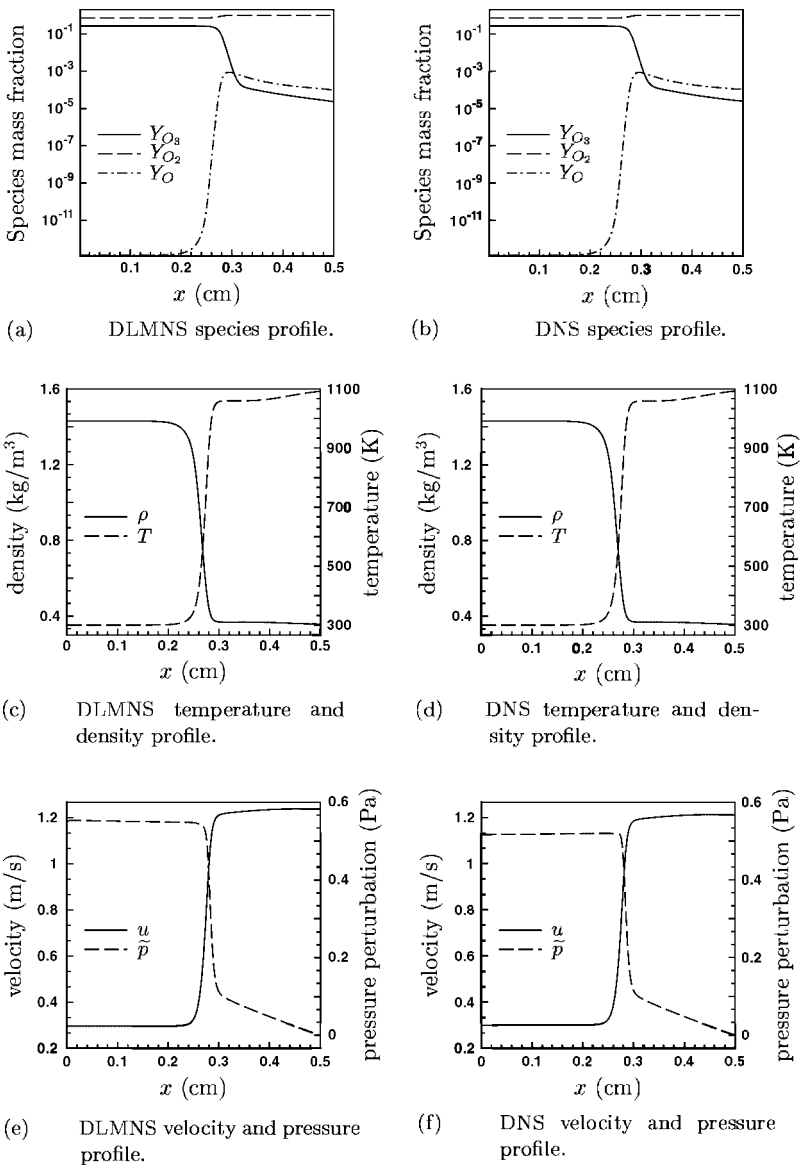

(a) DLMNS species profile. (b) DNS species profile.

(c) DLMNS temperature and density profile. (d) DNS temperature and density profile.

(e) DLMNS velocity and pressure profile. (f) DNS velocity and pressure profile.

Figure 3. Laminar one-dimensional ozone premixed flame computed with the DLMNS code (left) and the DNS code (right): (a) DLMNS species profile; (b) DNS species profile; (c) DLMNS temperature and density profile; (d) DNS temperature and density profile; (e) DLMNS velocity and pressure profile; (f) DNS velocity and pressure profile.

profiles. This initial turbulence corresponds to $u' = 1.09$ m/s and $\Lambda = 0.72$ mm, leading to a Reynolds number of 58. The computational domain is 5 mm long and 4 mm wide, with a grid size of 20 μm in both directions. The computation is periodic along the spanwise direction, the left boundary is an inlet and the right boundary an outlet.

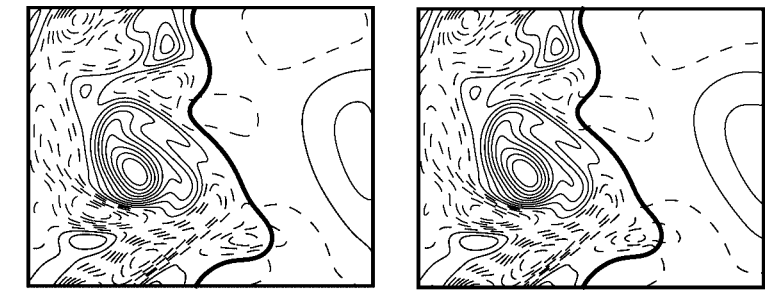

Figure 4. Isolevel of O_3 mass fraction $Y_{O_3}=0.05$ (bold solid line) and isolevels of vorticity (thin solid lines for positive values, thin dashed lines for negative values) at $t=2\tau$. Results obtained with the DNS code (a) and with the DLMNS code (b).

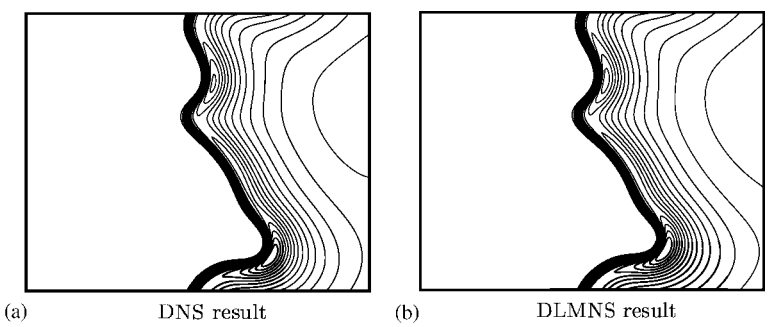

Figure 5. Isolevels of O mass fraction at $t=2\tau$. Results obtained with the DNS code (a) and with the DLMNS code (b).

The simulations have been again performed using the DNS code and the low-Mach number DLMNS code. The limiting time-step of the DNS code is $\Delta t=2.6\times10^{-8}$ s and corresponds to the classical acoustic CFL limitation (CFL$=0.8$). The Fourier criterion is the limiting diffusion stability condition for the DLMNS code and the corresponding time-step is $\Delta t=2\times10^{-7}$ s. In this configuration the time-step is therefore increased by a factor of 7, but we observe a reduction in computing time by a factor of 11 using the DLMNS code. This is due to the fact that these simulations have been performed on a highly vectorized supercomputer NEC-SX5, so that the computation time depends on the vectorization level of each code. The obtained vectorization is much better for the DLMNS code, thus explaining this larger acceleration factor.

The results obtained using the DNS and DLMNS codes at $t=2\tau$, where $\tau=0.66$ ms is the characteristic turbulence time, are shown in Figures 4 and 5. The flame shapes, shown by the black isolevel $Y_{O_3}=0.05$ (Figure 4), and the behaviour of the intermediate species O (Figure 5) are very close in both simulations. In particular, we observe that the concentration of the O radical is always higher in flame regions that are highly curved towards the burnt gases. This comparison clearly shows that the flame presents the same behaviour with the low-Mach number code and with the compressible one.

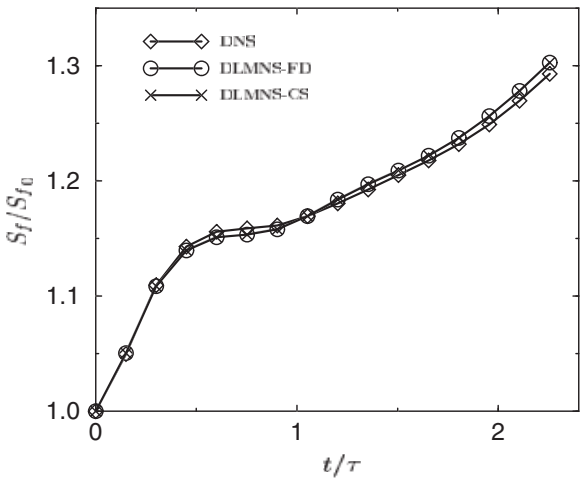

Figure 6. Time evolution of the flame surface area S_f normalized by the initial flame surface area S_{f_0}.

However, we observe some differences. The most striking one can be seen in the vorticity isolevels. The agreement in shape and absolute value is very satisfactory in the centre of the numerical domain. But noticeable differences appear close to the left and right boundaries. As in the one-dimensional case this can readily be explained by the different boundary conditions used in the DLMNS and DNS codes. In the compressible code acoustic waves can propagate through these boundaries, partial reflection can take place, and the resulting coupling between pressure and vorticity is much more complex than what is observed in the DLMNS code, where the Poisson equation for the pressure perturbation is only associated with simple Neumann and Dirichlet boundary conditions. Nevertheless, the low-Mach number formulation is clearly able to reproduce the advection of vorticity waves through the numerical domain, even in cases involving diffusion and reaction of chemical species.

The objective of such studies pertaining to flame/turbulence interaction is to investigate both local and global flame properties. To analyse the impact of the low-Mach number assumption, we also compute the time evolution of the flame surface S_f and the integrated heat-release rate H_r. The flame surface S_f is defined as the length of the isolevel $Y_{O_2} = 0.05$ and is normalized by its initial value S_{f_0}. The time evolution of S_f/S_{f_0} is shown in Figure 6. Here again the results of DLMNS and DNS are similar. The flame surface area first increases sharply as the strong initial turbulence interacts with the flame front. After one turbulence time ($t/\tau > 1$), the turbulence field is well established and still curves the flame front, so that the flame surface increases steadily but at a lower rate due to the viscous dissipation of turbulent structures. The global stretch rate $(1/S_f)\partial_t S_f$ is nearly constant. The integrated heat-release rate H_r normalized by its initial value H_{r_0} is plotted in Figure 7 and the same conclusions can be drawn as for the flame surface area. Here again the differences observed between the DNS and DLMNS results can be explained by the different behaviour at the boundaries and by the propagation of weak acoustics waves. It is possible to explain why the difference is smaller for S_f than for H_r. The flame front is located well inside the numerical domain and is therefore less sensitive to the boundary conditions than the heat release. For this latter quantity the influence of slight modifications in the burnt gas region, in particular near the right boundary, can slightly modify

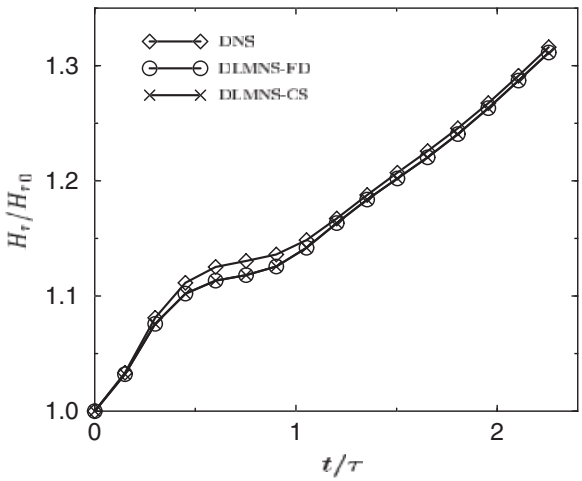

Figure 7. Time evolution of the integrated heat-release rate H_r normalized by the initial integrated heat-release rate H_{r_0}.

the integrated value. Anyway, for both global quantities, the difference between compressible and low-Mach formulations remains below 1%.

Two different discretizations of the same order, referenced as DLMNS-CS for the compact scheme and DLMNS-FD for the finite-difference scheme, have been used to solve the pressure Poisson equation (5) in the DLMNS approach. These two simulations lead to an identical velocity profile and flame shape. For comparison purposes we only show the time evolution of the flame surface area S_f and of the integrated heat-release rate H_r for these two discretizations in Figures 6 and 7. The agreement between both formulations of the pressure solver is perfect. It is well-known that compact schemes possess pseudo-spectral properties and are more suitable to perform accurate simulations. Since in the present DLMNS simulations the accuracy of the results is not improved by using the compact scheme, we conclude that the small discrepancies observed between the DNS and the DLMNS computations do not result from the method employed to solve the Poisson equation for pressure. This shows again that the different boundary conditions are mainly responsible for the observed discrepancies.

In order to check the local influence of the turbulence on the heat release, we define a simple progress variable c as

$$c = 1 - Y[O_3]/Y[O_3]_u$$

where $Y[O_3]$ is the local mass fraction of O_3 and $Y[O_3]_u$ is the mass fraction of O_3 in the unburnt gas. We plot the mean value and the root-mean-square of the local heat-release rate as a function of the progress variable c in Figure 8. The results presented are normalized by the same value, which corresponds to the maximum value of the local heat-release obtained in the one-dimensional laminar DNS simulation. We observe that the mean values from DLMNS are close to that from DNS. In the same way the root-mean-square of the local heat-release rate is comparable for the DNS and DLMNS computations. The fluctuation level due to turbulence is much higher than the difference between the two mean values, showing that the influence of

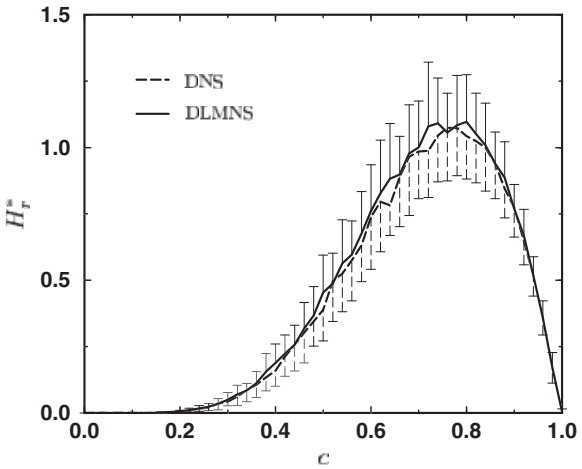

Figure 8. Local mean value (lines) and root-mean-square value (error bars) of the instantaneous normalized heat-release rate H_r^* versus the progress variable c for DNS (long dashed line and lower error bars) and DLMNS computations (solid line and upper error bars) at $t=2\tau$.

turbulence is much larger than the difference induced by the low-Mach number approximation itself.

We are currently working on similar comparisons for a H_2/O_2 flame. Hydrogen chemistry is much faster than ozone chemistry, requiring the use of an implicit treatment for the reactive terms in order to be able to really increase the time-step in DLMNS computations. Of course the comparison between DNS and DLMNS will be somewhat more difficult, since the structure of the DLMNS code must be modified to use an implicit integration step and will become different from that of the original, fully explicit DNS solver.

CONCLUSIONS

Starting from the compressible multi-species Navier–Stokes equations, we have explained in this paper how it is possible to modify these equations in the low-Mach number limit. The solution method employed in the low-Mach number case has been explained and we have fully implemented this method in a new code. We call this approach direct low-Mach number simulation. Results obtained with this code have been compared with those of direct numerical simulations relying on the compressible Navier–Stokes equations. The numerical methods employed for discretization and time-integration as well as the physical models describing chemical and transport processes are similar in both solvers. It is therefore possible to compare directly the obtained results, considering the DNS as a reference. Nevertheless, it must be kept in mind that the boundary conditions are necessarily different in these two codes.

We have first computed the time-dependent evolution of a field of homogeneous isotropic turbulence using both methods. The agreement between the two results is good, showing that the pressure/velocity coupling is accurately reproduced with the low-Mach number approximation.

In a second step we have investigated a turbulent premixed ozone flame. We have shown again that the flame behaviour is very well described by the low-Mach number assumption. The profiles of the main species and temperature are nearly identical to the DNS results. Nevertheless, some differences appear, in particular due to the fact that the configuration is non-periodic in one direction. Since the two codes employ very different boundary conditions, small differences appear at the boundaries and tend to modify global quantities such as the integrated heat-release rate. The evolutions of velocity, pressure and vorticity also show slight differences near the boundaries. But these variations are small compared to the magnitude of the physical fluctuations induced by turbulence. Since the origin of these differences is well-understood, they do not change the conclusion that the low-Mach number approximation can be used to investigate turbulent combustion with a good accuracy. Moreover, we observe that computing times can be typically reduced by an order of magnitude compared to direct simulations relying on the compressible equations.

We plan to investigate other reactive systems. In order to reach higher speed-ups, we are presently implementing an implicit integration of the reaction terms. We will then be able to compute turbulent hydrogen–air or methane–air flames using detailed reaction schemes while keeping reasonable computing times.

REFERENCES

1. Poinsot T, Veynante D, Candel S. Quenching processes and premixed turbulent combustion diagrams. *Journal of Fluid Mechanics* 1991; **228**:561–606.
2. Baum M, Poinsot T, Haworth DC, Darabiha N. Direct numerical simulation of $H_2/O_2/N_2$ flames with complex chemistry in two-dimensional turbulent flows. *Journal of Fluid Mechanics* 1994; **281**:1–32.
3. Poinsot T, Candel S, Trouvé A. Applications of direct numerical simulation to premixed turbulent combustion. *Progress in Energy Combustion Science* 1996; **21**:531–576.
4. Vervisch L, Veynante D. Direct numerical simulation of non-premixed turbulent flames. *Annual Review of Fluid Mechanics* 1998; **30**:655–691.
5. Maas U, Pope SB. Simplifying chemical kinetics: intrinsic low-dimensional manifolds in composition space. *Combustion and Flame* 1992; **88**:239–264.
6. Candel S, Thévenin D, Darabiha N, Veynante D. Progress in numerical combustion. *Combustion Science and Technology* 1999; **149**:297–337.
7. Prasad K, Interaction of pressure perturbations with premixed flames. *Combustion and Flame* 1994; **97**: 173–200.
8. O'Rourke PJ, Bracco FV. Two scaling transformations for the numerical computation of multidimensional unsteady laminar flames. *Journal of Computational Physics* 1979; **33**:185–203.
9. Ramshaw JD, O'Rourke PJ, Stein LR. Pressure gradient scaling method for fluid flow with nearly uniform pressure. *Journal of Computational Physics* 1985; **58**:361–376.
10. Jenny P, Müller B. Convergence acceleration for computing steady-state compressible flow at low-Mach numbers. *Computers and Fluids* 1999; **28**:951–972.
11. Cuenot B, Angelberger C, Legier J-P. Convergence acceleration for steady flame computations. *Journal of Computational Physics* 2000; **161**:718–722.
12. Chorin AJ, A numerical method for solving incompressible viscous flow problems. *Journal of Computational Physics* 1967; **2**:12–26.
13. Majda A, Sethian J. The derivation and numerical solution of the equations for zero Mach number combustion. *Combustion Science and Technology* 1985; **42**:185–205.
14. McMurtry PA, Jou W-H, Riley JJ, Metcalfe RW. Direct numerical simulations of a reacting mixing layer with chemical heat release. *AIAA Journal* 1986; **24**:962–970.
15. Katta VR, Goss LP, Roquemore WM. Effect of nonunity Lewis number and finite-rate chemistry on the dynamics of a hydrogen-air jet diffusion flame. *Combustion and Flame* 1994; **96**:60–74.
16. Katta VR, Roquemore WM, On the structure of stretched/compressed laminar flamelet–influence of preferential diffusion. *Combustion and Flame* 1995; **100**:61–70.
17. Nicoli C, Haldenwang P, Denet B. Ignition of a reactive mixing layer. *Journal de Chimie Physique* 1999; **96**:1016–1021.

18. Najm HN, Wyckoff PS, Knio OM. A semi-implicit numerical scheme for reacting flow. *Journal of Computational Physics* 1998; **143**:381–402.
19. Knio OM, Najm HN, Wyckoff PS. A semi-implicit numerical scheme for reacting flow II: stiff, operator-split formulation. *Journal of Computational Physics* 1999; **154**:428–467.
20. Kuo KK. *Principles of Combustion*. Wiley: New York, 1986.
21. Giovangigli V. *Multi-Component Flow Modeling*. Birkhäuser: Boston, 1999.
22. Kee RJ, Miller JA, Jefferson TH. CHEMKIN: a general-purpose, problem-independent, transportable, Fortran chemical-kinetics code package. *Technical Report* SAND80-8003, Sandia National Laboratories, 1980.
23. Maas U, Warnatz J. Simulation of chemically reacting flows in two-dimensional geometries. *Impact of Computers on Science and Engineering* 1989; **1**:394–420.
24. Ern A, Giovangigli V. *Multicomponent Transport Algorithms. New Series Monographs*, vol. 24. Lecture Notes in Physics. Springer: Heidelberg, 1994.
25. Ern A, Giovangigli V. Fast and accurate multicomponent transport property evaluation. *Journal of Computational Physics* 1995; **120**:105–116.
26. Ern A, Giovangigli V. Thermal diffusion effects in hydrogen–air and methane–air flames. *Combustion Theory and Modelling* 1998 **2**:349–372.
27. Volpe G. On the use and accuracy of compressible flow codes at low-Mach numbers. *AIAA Paper* 91-1662, 1991.
28. Pletcher RH. Chen K-H. On solving the compressible Navier–Stokes equation for unsteady flows at very low-Mach number. *AIAA Paper* 93-3368, 1993.
29. Nicoud F. Conservative high-order finite-difference schemes for low-Mach number flows. *Journal of Computational Physics* 2000; **158**:71–97.
30. Ben Dakhlia R, Giovangigli V. Multiradii modeling of counterflow spray diffusion flames. *Proceedings of the Combustion Institute* 2000; **28**:1039–1045.
31. Thévenin D, Behrendt F, Maas U, Przywara B, Warnatz J. Development of a parallel direct simulation code to investigate reactive flows. *Computers and Fluids* 1996; **25**:485–496.
32. Thévenin D, Renard P, Rolon J, Candel S. Extinction processes during a non-premixed flame/vortex interaction, *Proceedings of the Combustion Institution* 1998; **27**:719–726.
33. Baum M, Poinsot T, Thévenin D. Accurate boundary conditions for multicomponent reactive flows. *Journal of Computational Physics* 1994; **116**:247–261.
34. Swarztrauber PN. In *Parallel Computations*, Rodrigue, G (ed.). Academic Press: New York, 1982; 51–83.
35. Lele SK. Compact finite difference schemes with spectral-like resolution. *Journal of Computational Physics* 1992; **103**:16–42.
36. Cook AW, Riley JJ. Direct numerical simulation of a turbulent reactive plume on a parallel computer. *Journal of Computational Physics* 1996; **129**:263–283.
37. Kincaid DR. Cheney EW. *The Mathematics of Scientific Computing*. Brooks/Cole Publishers: Dublin, 1990.
38. Roache PJ. A sixth-order accurate direct solver for the Poisson and Helmholtz equations. *AIAA Journal* 1979; **17**:524–526.
39. Roache P. *Fundamentals of Computational Fluid Dynamics*. Hermosa Publisher: Albuquerque, 1998.
40. Hinze JO. *Turbulence*. McGraw-Hill: New York, 2nd ed., 1975.
41. Lesieur M. *Turbulence in Fluids*. Kluwer Academic Publishers: Dordrecht, 2nd ed., 1990.
42. Brachet ME, Meneguzzi M, Politano H, Sulem PL. The dynamics of freely decaying two-dimensional turbulence. *Journal of Fluid Mechanics* 1988; **194**:333–349.
43. Karlin V, Makhviladze G, Roberts J. In *Sixteenth International Conference on Numerical Methods in Fluid Dynamics*, Bruneau C-H (ed.). Springer: Berlin, 1998, 500–505.
44. Jackson TL, Macaraeg MG, Hussaini MY. The role of acoustics in flame/vortex interactions. *Journal of Fluid Mechanics* 1993; **254**:579–603.
45. Warnatz J. Calculation of the structure of laminar flat flames I: flame velocity of freely propagating ozone decomposition flames. *Berichte Bunsenges. Physics Chemistry* 1978; **82**:193–200.
46. Coffee TP, Kotlar AJ, Miller MS. The overall reaction concept in premixed, laminar, steady-state flames. I. Stoichiometries. *Combustion and Flame* 1983; **54**:155–169.

